Pearson et al., http://www.jcb.org/cgi/content/full/jcb.200908019/DC1

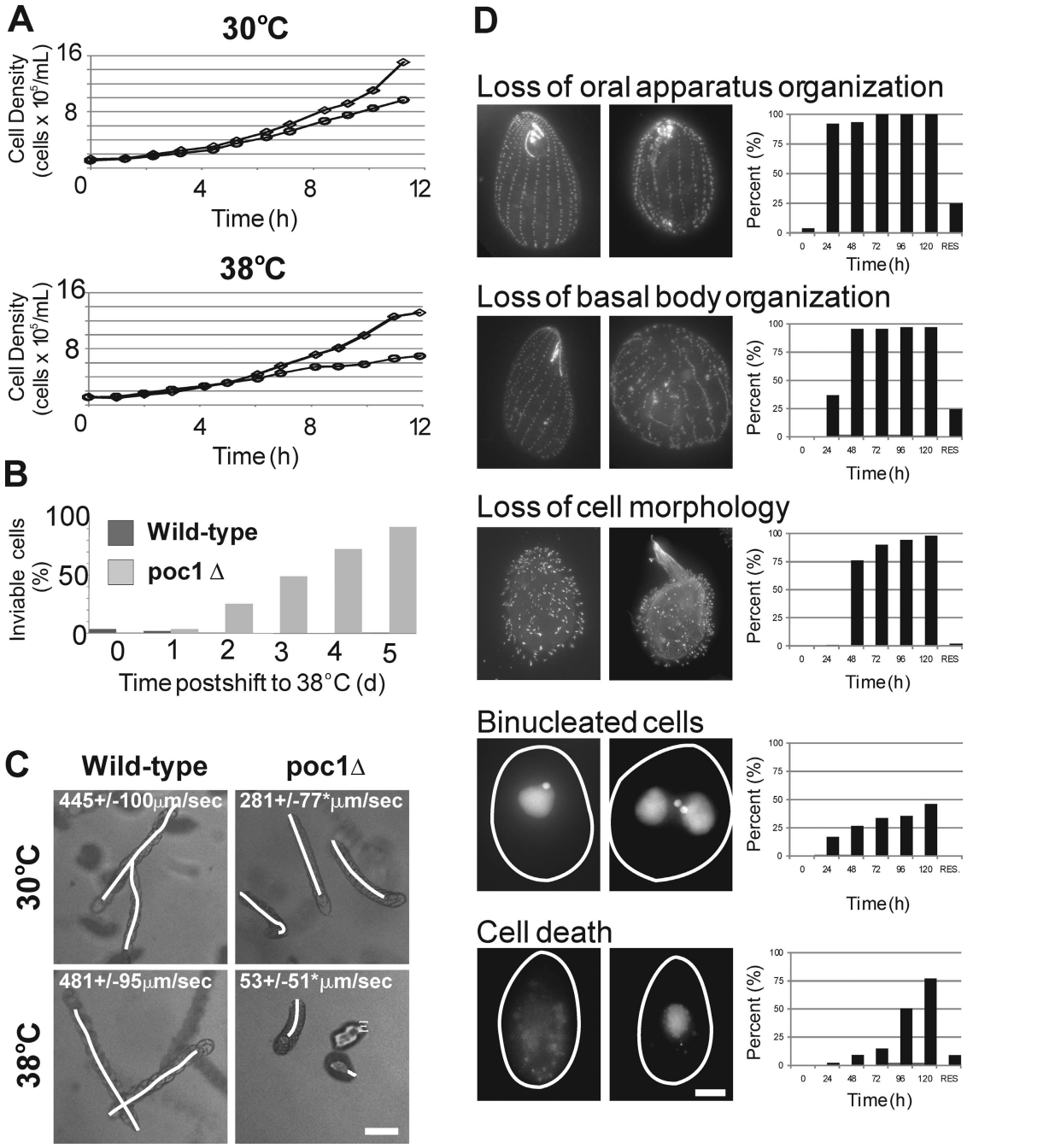

Figure S1. **Growth, swimming, and morphological defects in *poc1Δ*.** (A) Representative cell growth curve for wild-type cells (diamonds) and *poc1Δ* knockout cells (ovals). At 38°C, *poc1Δ* cell densities leveled, and no additional increase was observed ($n = 3$). (B) *poc1Δ* cells exhibited a time-dependent increase in cell death after shifting cells to 38°C. (C) Poc1 loss causes decreased swimming rates. Representative panels are projections of 10 image planes equivalent to 0.45 s of total imaging time. Movement is evident by shifts in the cell position along the swimming path, and white lines indicate the motility path. Mean swimming rates are provided on the top left of each panel. Cells were shifted to 38°C for 16 h. *, $P < 0.01$; $n = 200$ cells. Bar, 50 µm. (D) Cellular phenotypes were quantified for *POC1* wild-type and *poc1Δ* cells at 38°C. The observed phenotypes include loss or disorganization of the oral apparatus (anticentrin), basal body disorganization (anticentrin), loss of cell morphology (anti–α-tubulin), binucleated cells (DNA; Hoescht 33342), and cell death (propidium iodide uptake). Left panels and gray bars represent wild-type cells, and right panels and black bars represent *poc1Δ* cells. The rescue column (RES) describes each phenotype in *poc1Δ* cells with GFP-Poc1 rescue at 38°C for 120 h. $n = 100$ cells for each condition. Bar, 10 µm.

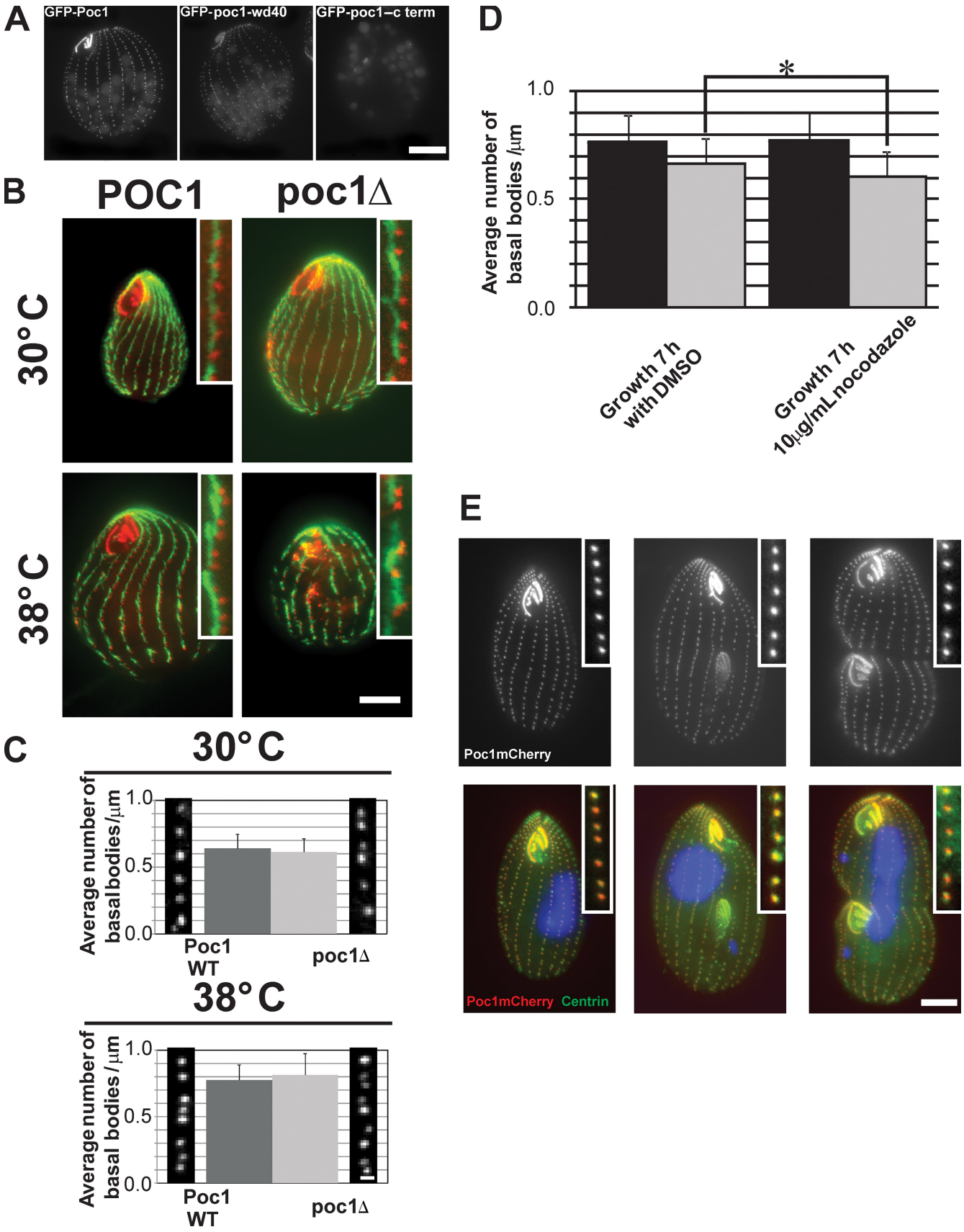

Figure S2. **Poc1 localization and basal body frequency.** (A) Fluorescence localization of GFP-Poc1, GFP-poc1-wd40, and GFP-poc1–c terminus. A fusion containing only the N-terminal 342 aa (including the WD40 repeat) localized to basal bodies, as found for the full-length protein. However, the C-terminal fusion did not localize to basal bodies. Relative fluorescence intensities (arbitrary units) are as follows: 100 ± 20.5, 76.5 ± 11.9, and 0.0 ± 0.0 (*n* >

350 basal bodies). Cellular GFP fluorescence was evident in all conditions tested. Bar, 10 µm. (B) Kinetodesmal fibers extend from basal bodies in *poc1Δ* cells at both temperatures. *poc1Δ* cells were grown at 30°C and 38°C for 24 h before staining with antirootlet (green) and anticentrin (red) to visualize kinetodesmal fibers and basal bodies, respectively. Insets show a magnified view. Bar, 10 µm. (C) Cells were grown for 24 h, and the frequency of basal bodies (anticentrin) per micrometer was quantified. Basal bodies were counted in the medial region of interphase cells. Basal body frequencies are similar in cells grown at a constant temperature, and the number of basal bodies increases significantly when comparing cells grown at either 30 (*poc1Δ*, 0.61 ± 0.11 bb/µm; *POC1*, 0.64 ± 0.11 bb/µm) or 38°C (*poc1Δ*, 0.82 ± 0.16 bb/µm; *POC1*, 0.78 ± 0.12 bb/µm) for 24 h ($P < 0.001$; $n > 150$). Insets represent the basal body frequency for a 10-µm segment of the medial ciliary row of interphase cells. WT, wild type. Bar, 1 µm. (D) Basal bodies in *poc1Δ* cells are sensitive to nocodazole. Wild-type (black bars) and *poc1Δ* (gray bars) cells were grown at 30°C in 10 µg/ml nocodazole for 7 h. The frequency of basal bodies was significantly decreased in *poc1Δ* cells compared with wild-type (with nocodazole: *poc1Δ*, 0.61 ± 0.14 bb/µm; *POC1*, 0.77 ± 0.12 bb/µm; without nocodazole: *poc1Δ*, 0.66 ± 0.13 bb/µm; *POC1*, 0.76 ± 0.11 bb/µm; $n > 300$). To quantify cells in the same cell cycle phase, only cells in early cell division (oral primordium stages 1 and 2) were quantified. (E) Endogenous *T. thermophila* Poc1 localizes to basal bodies. Endogenous Poc1 fused to mCherry fluorescent protein (red) at the C terminus was imaged relative to basal bodies (green; anticentrin) and DNA (blue; Hoescht 33342). Poc1 and centrin colocalize at basal bodies. Interphase (left), early cell division (middle), and late cell division (right) are shown. Insets show a magnified view. Bar, 10 µm. *, $P < 0.01$. Error bars indicate mean ± SD.

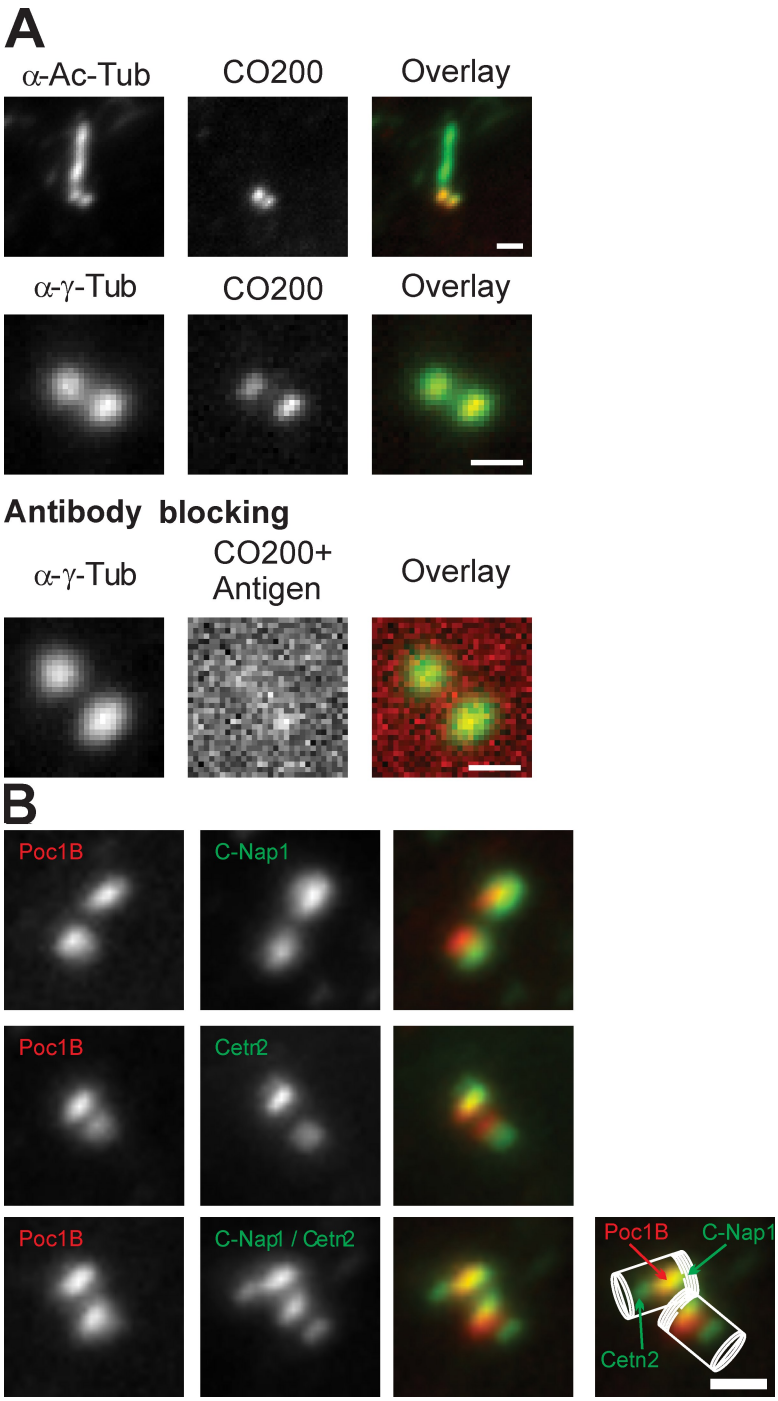

Figure S3. **Endogenous human Poc1B localizes to basal bodies and centrioles.** (A) Antibodies to HsPoc1B (CO200) target basal bodies and centrioles. Images represent localization of HsPoc1B (red) relative to basal bodies and primary cilia (acetylated tubulin; top, green) and centrosomes (γ-tubulin; middle and bottom, green). Preincubation of α-HsPoc1B with HsPoc1B antigen before immunofluorescence blocked antibody recognition of centrioles (bottom) and basal bodies (not depicted). (B) HsPoc1B localizes to the proximal end of centrioles of U2OS cells. Poc1B (CO200) was colocalized relative to C-Nap1 (basal body proximal end marker) and centrin (Cetn2; distal lumen marker). Bar, 1 μm.

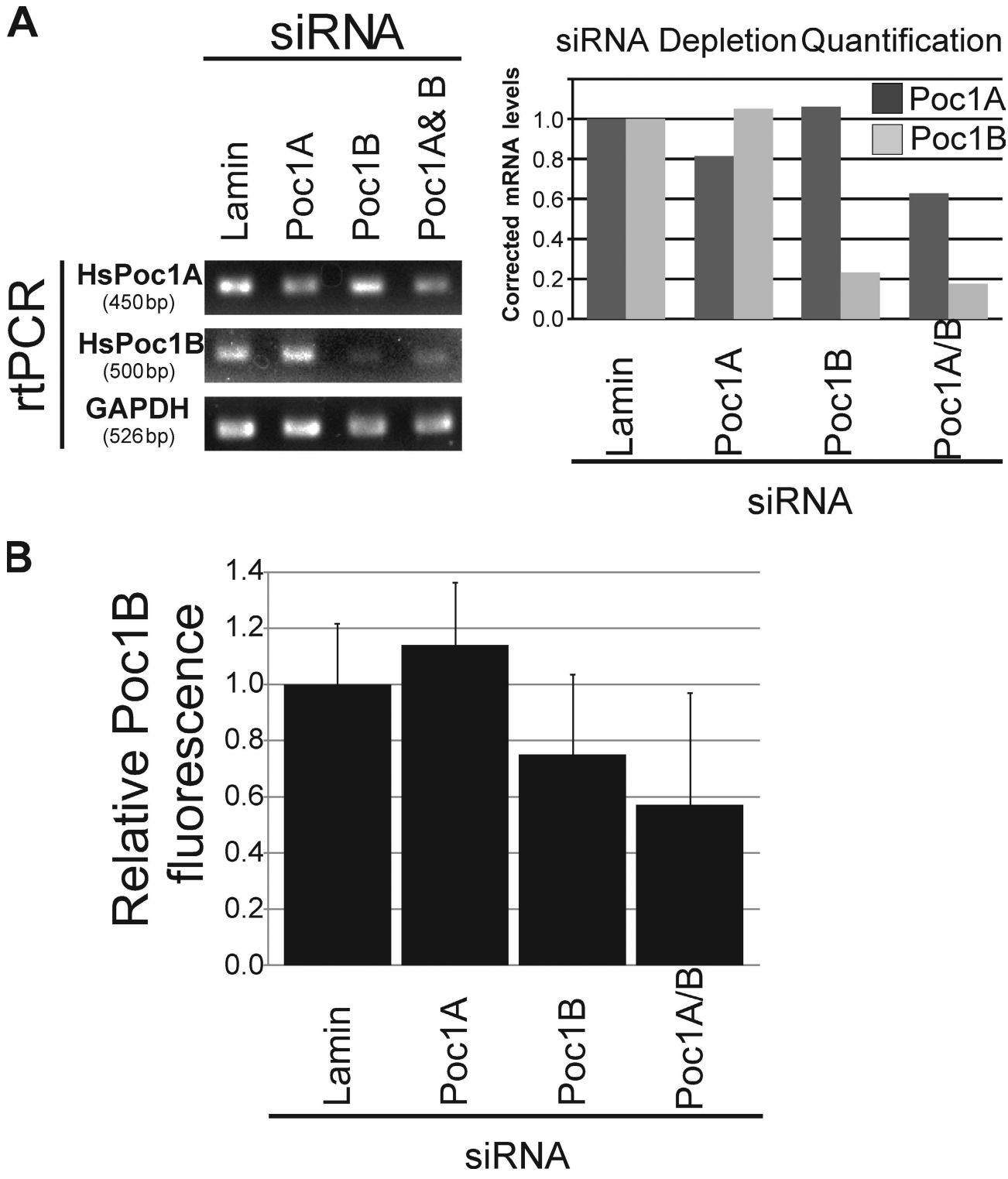

Figure S4. **siRNA depletion of HsPoc1A and HsPoc1B.** (A) HsPoc1A and HsPoc1B mRNA depletion was measured using RT-PCR of total RNA from RPE-1 cells induced for ciliogenesis. HsPoc1A, HsPoc1B, and GAPDH mRNA levels were measured under each siRNA condition. Quantified mRNA levels were corrected based on GAPDH control levels. Data shown are representative of three experiments. (B) The basal body/centriole fluorescence signal of Poc1B was measured using anti-Poc1B antibodies (CO200). A significant drop in fluorescence was observed in the HsPoc1B siRNA-treated cells ($P < 0.001$). $n > 75$ centrioles for each condition. Error bars indicate mean ± SD.

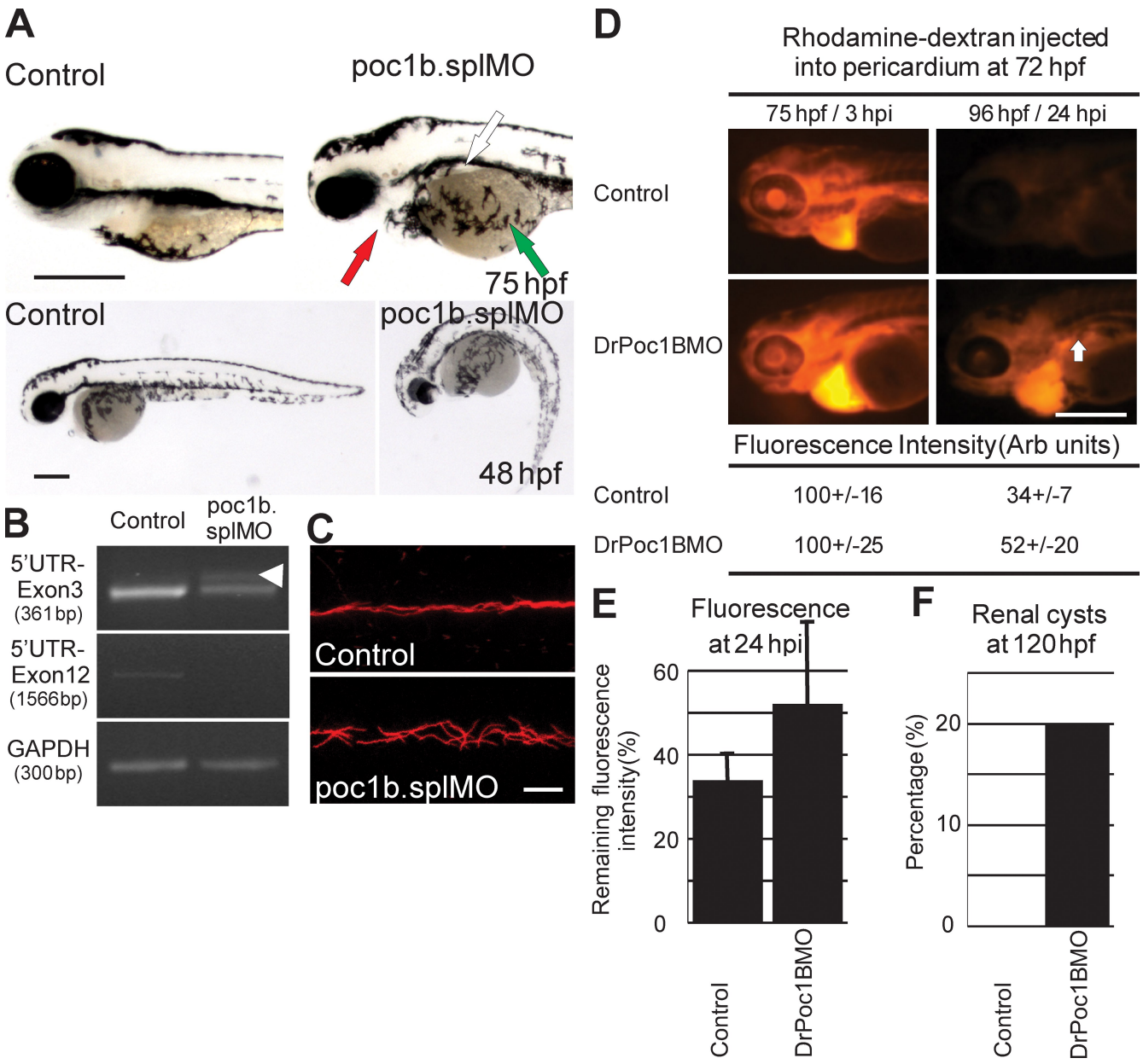

Figure S5. **Defective renal clearance and increased kidney cysts in Poc1B morphants.** (A) To verify that the phenotype observed with *Dr.poc1b* MO was caused by specific knockdown of Poc1B, a second MO was designed to target the *Dr.poc1b* intron 1–exon 2 splice site (*Dr.poc1b.splMO*). Similar to results observed with the *Dr.poc1b MO*, *Dr.poc1b.splMO* morphants showed common ciliopathy traits: heart edemas (red arrow), pronephric cysts (white arrow), small eyes, irregular melanocyte migration (green arrow), and curly tails. Bars, 0.5 mm. (B) DrPoc1B knockdown was confirmed by RT-PCR of 48-hpf embryos, and primers were used against the full-length transcript (5′ untranslated region/exon 12) and a shorter product surrounding intron 1 (5′ untranslated region/exon 3). *Dr.poc1b.spl* morphants showed a reduction in the endogenous *POC1B* species and an additional modified, larger transcript (arrowhead). The full-length *POC1B* PCR product was observed in control but not morphant RNA extracts, which is suggestive of nonsense RNA-mediated decay. GAPDH served as a loading control. (C) Consistent with a role in ciliogenesis, *Dr.poc1b.spl* morphants displayed disorganized motile cilia in the pronephric ducts. Bar, 10 µm. (D) To quantify the efficiency of renal clearance, rhodamine–dextran (10 kD) was injected into the pericardium of 72-hpf zebrafish, and clearance from the entire fish was quantified. Rhodamine fluorescence intensities in the pericardium were measured at 3 (75 hpf) and 24 h post injection (hpi; 96 hpf). Images display representative fluorescence for control and DrPoc1B MO–injected (DrPoc1B MO) fish. Arrow indicates poor excretion of fluorescence from the pronephretic ducts. The relative fluorescence intensity in the pericardium is displayed in the table (n = 10). Bar, 0.5 mm. (E) The relative fluorescence clearance between the control and *Dr.poc1b* MO–injected zebrafish was quantified. *Dr.poc1b* MO injection resulted in decreased efficiency of rhodamine–dextran clearance (n = 10). (F) The presence of kidney cysts was quantified in these same fish at 120 hpf. A 20% increase in the frequency of kidney cysts was found for *Dr.poc1b* MO (n = 10). Error bars indicate mean ± SD.